A

B

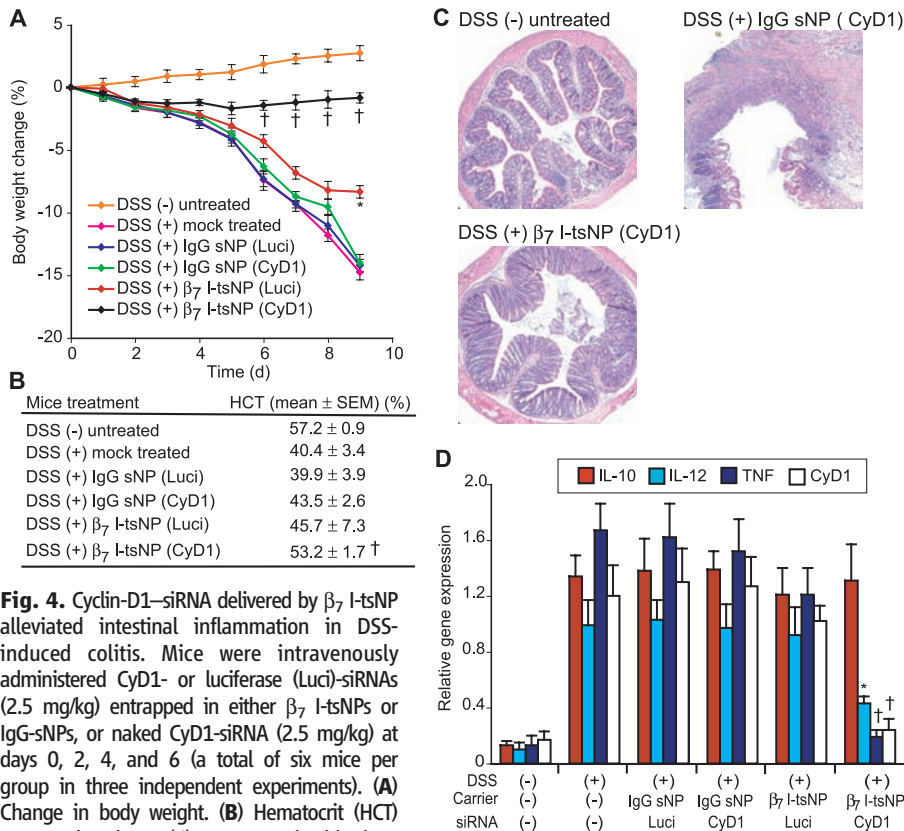| Mice treatment	HCT (mean ± SEM) (%)
DSS (−) untreated	57.2 ± 0.9
DSS (+) mock treated	40.4 ± 3.4
DSS (+) IgG sNP (Luci)	39.9 ± 3.9
DSS (+) IgG sNP (CyD1)	43.5 ± 2.6
DSS (+) β₇ I-tsNP (Luci)	45.7 ± 7.3
DSS (+) β₇ I-tsNP (CyD1)	53.2 ± 1.7 †

C

D

Fig. 4. Cyclin-D1–siRNA delivered by β_7 I-tsNP alleviated intestinal inflammation in DSS-induced colitis. Mice were intravenously administered CyD1- or luciferase (Luci)-siRNAs (2.5 mg/kg) entrapped in either β_7 I-tsNPs or IgG-sNPs, or naked CyD1-siRNA (2.5 mg/kg) at days 0, 2, 4, and 6 (a total of six mice per group in three independent experiments). (**A**) Change in body weight. (**B**) Hematocrit (HCT) measured at day 9. (**C**) Representative histology at day 9 (hematoxylin and eosin staining, magnification ×100). (**D**) mRNA expression of CyD1 and cytokines in the gut. mRNA expression was measured by qRT-PCR with homogenized colon samples harvested at day 9. (A), (B), and (D) Data are expressed as the mean ± SEM of three independent experiments. *$P < 0.05$, †$P < 0.01$ versus mock-treated mice with DSS-induced colitis.

body targets for both delivery and uptake of tsNPs. Thus, the I-tsNP approach may have broad applications not only for in vivo drug target validation, but also for potential therapies that are not limited to leukocytes or inflammatory settings.

References and Notes
1. E. Iorns, C. J. Lord, N. Turner, A. Ashworth, *Nat. Rev. Drug Discov.* **6**, 556 (2007).
2. D. W. Stacey, *Curr. Opin. Cell Biol.* **15**, 158 (2003).
3. M. Fu, C. Wang, Z. Li, T. Sakamaki, R. G. Pestell, *Endocrinology* **145**, 5439 (2004).
4. R. Yang, W. Bie, A. Haegebarth, A. L. Tyner, *Cell Cycle* **5**, 180 (2006).
5. H. van Dekken et al., *Acta Histochem.* **109**, 266 (2007).
6. M. A. Behlke, *Mol. Ther.* **13**, 644 (2006).
7. D. M. Dykxhoorn, J. Lieberman, *Annu. Rev. Biomed. Eng.* **8**, 377 (2006).
8. D. Peer, P. Zhu, C. V. Carman, J. Lieberman, M. Shimaoka, *Proc. Natl. Acad. Sci. U.S.A.* **104**, 4095 (2007).
9. Materials and methods are available as supporting material on *Science* Online.
10. C. R. Dass, *J. Mol. Med.* **82**, 579 (2004).
11. D. Peer, A. Florentin, R. Margalit, *Biochim. Biophys. Acta* **1612**, 76 (2003).
12. D. P. Andrew et al., *J. Immunol.* **153**, 3847 (1994).
13. S. K. Shaw, M. B. Brenner, *Semin. Immunol.* **7**, 335 (1995).
14. F. L. Sorgi, S. Bhattacharya, L. Huang, *Gene Ther.* **4**, 961 (1997).
15. S. D. Li, L. Huang, *Mol. Pharm.* **3**, 579 (2006).
16. J. O. Lindsay, A. Sandison, P. Cohen, F. M. Brennan, H. J. Hodgson, *Dig. Dis. Sci.* **49**, 1327 (2004).
17. J. Soutschek et al., *Nature* **432**, 173 (2004).
18. D. V. Morrissey et al., *Nat. Biotechnol.* **23**, 1002 (2005).
19. R. M. Schiffelers et al., *Nucleic Acids Res.* **32**, e149 (2004).
20. E. Song et al., *Nat. Biotechnol.* **23**, 709 (2005).
21. F. Takeshita et al., *Proc. Natl. Acad. Sci. U.S.A.* **102**, 12177 (2005).
22. J. D. Heidel et al., *Proc. Natl. Acad. Sci. U.S.A.* **104**, 5715 (2007).
23. We thank J. Lieberman for critically reading manuscript and discussion; R. Margalit, R. S. Langer, and P. Sicinski for discussions; and Y. Imai, A. Zur, P. Sage, and R. Yoo for technical assistance. D.P. is supported by the Dorot Foundation and Pfizer Inc. Y.M. is supported by the Uehara Memorial Foundation. This work was supported by the Arthritis Foundation (C.V.C.) and NIH grants HL048675 and AI63421 (M.S.).

Direct Observation of Hierarchical Folding in Single Riboswitch Aptamers

William J. Greenleaf,[1]* Kirsten L. Frieda,[2] Daniel A. N. Foster,[4] Michael T. Woodside,[4,5]*† Steven M. Block[1,3]†

Riboswitches regulate genes through structural changes in ligand-binding RNA aptamers. With the use of an optical-trapping assay based on in situ transcription by a molecule of RNA polymerase, single nascent RNAs containing *pbuE* adenine riboswitch aptamers were unfolded and refolded. Multiple folding states were characterized by means of both force-extension curves and folding trajectories under constant force by measuring the molecular contour length, kinetics, and energetics with and without adenine. Distinct folding steps correlated with the formation of key secondary or tertiary structures and with ligand binding. Adenine-induced stabilization of the weakest helix in the aptamer, the mechanical switch underlying regulatory action, was observed directly. These results provide an integrated view of hierarchical folding in an aptamer, demonstrating how complex folding can be resolved into constituent parts, and supply further insights into tertiary structure formation.

Riboswitches are elements of mRNA that regulate gene expression through ligand-induced changes in mRNA secondary or tertiary structure (*1*, *2*). This regulation is accomplished through the binding of a small metabolite to an aptamer in the 5′-untranslated region of the mRNA, which causes conformational changes that alter the expression of downstream genes.

Riboswitch-dependent regulatory processes depend crucially on the properties of aptamer folding; the kinetics and thermodynamics of folding are therefore of central importance for understanding function.

Among the simplest riboswitches are those regulating purine metabolism, which have aptamers with "tuning fork" structures (*3*, *4*) that bind ligands at a specific residue in a pocket formed by a three-helix junction. The junction is thought to be preorganized by numerous tertiary contacts, including interactions between two hairpin loops, but the binding pocket itself is likely stabilized only upon ligand binding (*4–10*). Ligand binding also stabilizes a nearby helix (*3–5*), sequestering residues that would otherwise participate in an alternate structure affecting gene expression (e.g., terminator or anti-terminator hairpins, ribosome binding sequences). Features such as ligand specificity (*6*, *11*) and its structural basis (*6*, *7*), the rates and energies for ligand binding and dissociation (*12*), the kinetics of loop-loop formation (*10*), and the interplay of structural preorganization and induced fit (*7–9*) have recently been investigated. These studies, how-

ever, focused on isolated steps in folding, typically using ligand analogs or investigating aptamers from different organisms. Here we obtain, from a single set of measurements, an integrated picture of secondary and tertiary structure formation, as well as ligand binding, in the aptamer of the *pbuE* adenine riboswitch from *Bacillus subtilis*, by observing folding and unfolding trajectories of individual molecules subjected to controlled loads in a high-resolution, dual-trap optical tweezers apparatus (*13*).

Single-molecule force spectroscopy, which measures the extension of a molecule as it unfolds and refolds under tension, furnishes a tool for probing structural transitions: Extension changes can be related to the number of nucleotides involved in folding. Furthermore, the effects of force on reaction equilibria and kinetics allow the shapes of the folding landscapes to be determined in detail (*14–16*). The complete folding process, starting from a fully unfolded state (not usually probed in conventional RNA folding studies), can also be observed. This initial configuration is especially relevant to riboswitches, because aptamers fold cotranscriptionally from an initially unstructured state. Because of the tight coupling between folding and transcription, the assay was designed to measure folding of mRNA transcribed in situ (*17*). A single *Escherichia coli* RNA polymerase (RNAP) molecule, transcriptionally stalled downstream of the promoter region on a DNA template (Fig. 1A), was attached to a bead held in one optical trap (Fig. 1B). The 29-nucleotide (nt) initial RNA transcript emerging from the RNAP was hybridized to the complementary cohesive end of a 3-kb double-stranded DNA (dsDNA) "handle" attached to a bead held in the other trap, creating a "dumbbell" geometry that allowed forces to be applied between the RNAP and the 5′ end of the RNA (*18*). Force-extension curves (FECs), showing the molecular extension measured as a function of force as the traps were moved apart at a constant rate, confirmed that this initial transcript was unstructured (Fig. 1C).

After constructing the dumbbells, transcription was restarted by introducing nucleoside triphosphates. The DNA template coded for the *pbuE* adenine riboswitch aptamer downstream of the initial transcript (Fig. 1A). Once the aptamer sequence was transcribed, RNAP was prevented from further elongation by a roadblock consisting of a streptavidin molecule bound to a 5′-terminal biotin label on the template (Fig. 1D). FECs measured immediately after aptamer transcription (Fig. 1E) revealed a characteristic series of sawtooth features that arise from contour length increases as specific structural

elements unfold (*19*). In the absence of adenine, two small unfolding events were typically observed (Fig. 1E, black). These features are produced by the unfolding of the two stable hairpins in the secondary structure, P3 and P2 (Fig. 1E, inset). The interactions that underpin tertiary structure by holding these hairpin loops together and structuring the binding pocket in the triple-helix junction are present only transiently in the absence of adenine (*5, 8, 10*). The contour length changes associated with these features, 17 ± 2 nt (P3) and 22 ± 2 nt (P2), are consistent with the values expected for these hairpins (19 and 21 nt, respectively) (*18*). In the presence of adenine, some FECs were identical to those observed in its absence, indicating in these cases that adenine was not bound to the aptamer. More commonly, however, larger unfolding distances at higher forces were observed, corresponding to adenine-induced stabilization of the folded structure. In the latter case, the aptamer usually unfolded cooperatively in a single event (Fig. 1E, blue), but sometimes through an intermediate state (Fig. 1E, red).

Unfolding from the fully folded state was analyzed in more detail by collecting multiple FECs from the same molecule. Overlaying 800 FECs shows that the aptamer unfolds over a wide distribution of forces (Fig. 2A), as expected for a nonequilibrium measurement (*20*). Three states were clearly seen: the folded and unfolded states, and an intermediate state. We fit the FECs with two worm-

like chains (WLCs) in series: one for the dsDNA handle (*21*) and the other for the single-stranded RNA (*22*), assuming a contour length of 0.59 nm/nt for RNA (*23*). When the aptamer unfolded fully, 62 ± 1 nt were released (*18*), in agreement with the 63-nt aptamer length. The intermediate state is 23 ± 1 nt shorter than the unfolded state, suggesting that it corresponds to a folded 21-nt P2 helix. The equilibrium free energy of the aptamer, computed by the method of Jarzynski (*24, 25*) from the nonequilibrium work done to unfold it (fig. S2), is 18 ± 2 kcal/mol (*18*). For comparison, the free energy predicted for the secondary structure in Fig. 1E is only ~12 ± 1 kcal/mol (*10*), indicating that tertiary contacts and ligand binding stabilize the aptamer by an additional ~6 ± 2 kcal/mol, in reasonable agreement with earlier measurements of the binding energy of 2-aminopurine (2AP), an adenine analog (*12*).

The distribution of forces, $p(F)$, for unfolding the fully folded aptamer (Fig. 2B) is well fit by an expression derived by Dudko *et al.* (*20*) for unfolding at fixed loading rate, parameterized by k_{off}, the unfolding rate at $F = 0$; $\Delta x^{\ddagger}$, the distance to the transition state from the folded state; and $\Delta G^{\ddagger}$, the height of the energy barrier (*18*). More than 3000 FECs measured for eight molecules, at loading rates varying from ~10 to 200 pN/s, yielded an unfolding rate $k_{off} \sim 0.04$ s^{-1} (ln $k_{off} = -3.5 \pm 1$), similar to the value of 0.15 s^{-1} measured previously by bulk kinetic methods (*12*). The activation
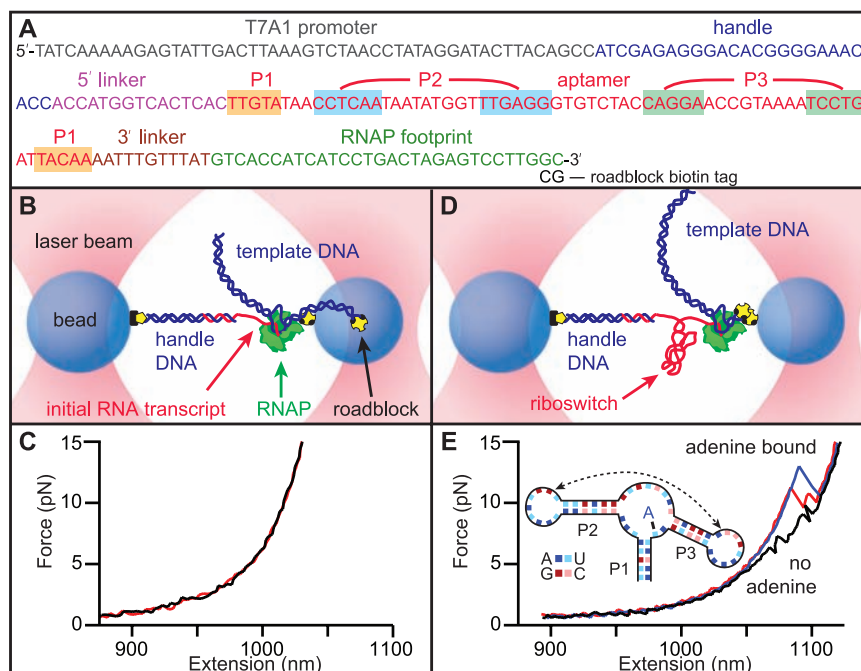

Fig. 1. (A) DNA template used for RNA transcription, showing the sequence of the nontranscribed promoter, the 25-bp section hybridizing with the DNA handle, the *pbuE* riboswitch aptamer (base-paired helices highlighted) flanked by short linkers, and the footprint of RNAP when stalled by the terminal roadblock. **(B)** Schematic of the optical trapping assay showing experimental geometry, with stalled RNAP and initial RNA transcript hybridized to the dsDNA handle (not to scale). **(C)** Two FECs obtained before aptamer transcription show little or no structure in the initial transcript. **(D)** Template DNA is transcribed in situ, producing an aptamer transcript, after which RNAP is stalled by a streptavidin molecule bound to the biotin-based roadblock. **(E)** FECs obtained after transcription show unfolding transitions in the aptamer. Without adenine, two events are seen (black), corresponding to the unfolding of hairpins P2 and P3 (inset). With adenine bound to the aptamer, larger unfolding events are observed (blue), sometimes involving an intermediate state (red).

[1]Department of Applied Physics, Stanford University, Stanford, CA 94305, USA. [2]Biophysics Program, Stanford University, Stanford, CA 94305, USA. [3]Department of Biological Sciences, Stanford University, Stanford, CA 94305, USA. [4]Department of Physics, University of Alberta, Edmonton AB, T6G 2G7, Canada. [5]National Institute for Nanotechnology, National Research Council of Canada, Edmonton AB, T6G 2M9, Canada.

*These authors contributed equally to this work.
†To whom correspondence should be addressed. E-mail: sblock@stanford.edu (S.M.B); michael.woodside@nrc.ca (M.T.W.)

energy, $\Delta G^{\ddagger}$, was 17 ± 4 kcal/mol, in agreement with a previous result for the unbinding of 2AP (*12*). The distance to the transition state $\Delta x^{\ddagger}$ was 2.1 ± 0.2 nm. Given an extension of ~0.42 nm/nt at the average unfolding force of ~15 pN, this result indicates that the transition state involves the unzipping of ~2.5 base pairs (bp) in helix P1, suggesting that the G:C base pair in P1 (Fig. 1E, inset) represents a structural keystone: Both the binding pocket and triple-helix junction unfold once it is disrupted. Isolated G:C base pairs located 3 to 4 bp from the loop of P1 are found in the other purine

riboswitches, suggesting that they may be an important structural feature of this class of aptamers.

The kinetics of refolding and ligand binding were probed by observing the fraction of FECs showing the unfolding signature of the fully folded, adenine-bound aptamer, as a function of adenine concentration and the variable time interval during which refolding could occur between successive measurements (Fig. 3). We fit these data to a minimal, two-step model (Fig. 3, inset): formation of an intermediate structure competent to bind adenine (taken to be effectively irreversible) followed by

adenine binding. The complete folding process involves a hierarchy of several steps, including folding of the three helices, formation of the loop-loop contacts and the adenine binding pocket, and binding of adenine. At $F = 0$, however, helix formation should be fast compared to formation of the tertiary
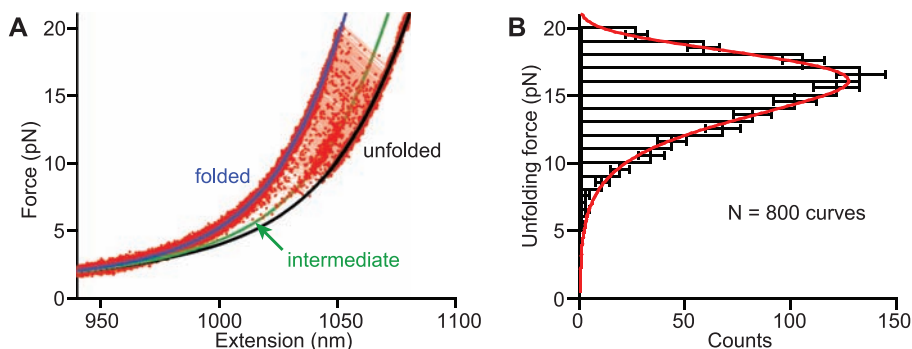

Fig. 3. Kinetics of aptamer refolding and binding. The fraction of FECs corresponding to the fully folded, adenine-bound aptamer (identified by the appropriate unfolding signature) for various adenine concentrations as a function of the variable time delay for refolding between pulls. Solid curves display the global fit to a minimal three-state kinetic scheme (**inset**): U, unfolded; A-comp, competent to bind adenine; F, folded (adenine-bound aptamer).

Fig. 2. (**A**) Nonequilibrium FECs for folded aptamer display a wide distribution of unfolding forces. WLC fit to the folded state (blue), and double WLC fits to the intermediate (green) and unfolded (black) states, indicate contour length changes of 39 ± 1 nt and 62 ± 1 nt for unfolding to the intermediate and unfolded states, respectively. (**B**) The unfolding force distribution is fit by a model returning the unfolding rate, along with the location and height of the energy barrier to unfolding.
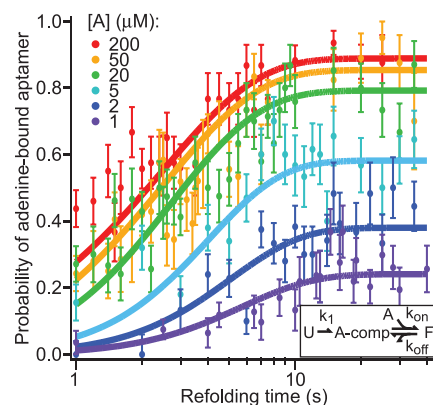
Fig. 4. Aptamer states and energetics determined by refolding at constant force. (**A**) As force is reduced, first P2 refolds (red), then P3 folds (orange). At lower forces, P2 and P3 interact to form a binding pocket and adenine binds, generating two additional states (green). The adenine-bound state is stable over many seconds, even at 5 pN load (blue). (**B**) Histograms of complete trajectories at different forces, with extension changes scaled by the force-dependent extension per nucleotide. Dashed lines indicate distinct states; the A-comp state is rarely populated. (**C** and **D**) Refolding trajectory and histograms in the absence of adenine. P2 and P3 folding occur as with adenine, but the A-comp state is highly populated at low force, whereas the folded state is very unstable, even at low force (purple). (**E**) Quantitative energy landscapes for aptamer folding at 6.5 pN, reconstructed from the experimental data in the presence (red) and absence (black) of adenine. The five potential wells correspond to five observed folding states, illustrated by cartoons. Adenine binding only appreciably affects the barrier and energy of the folded state.
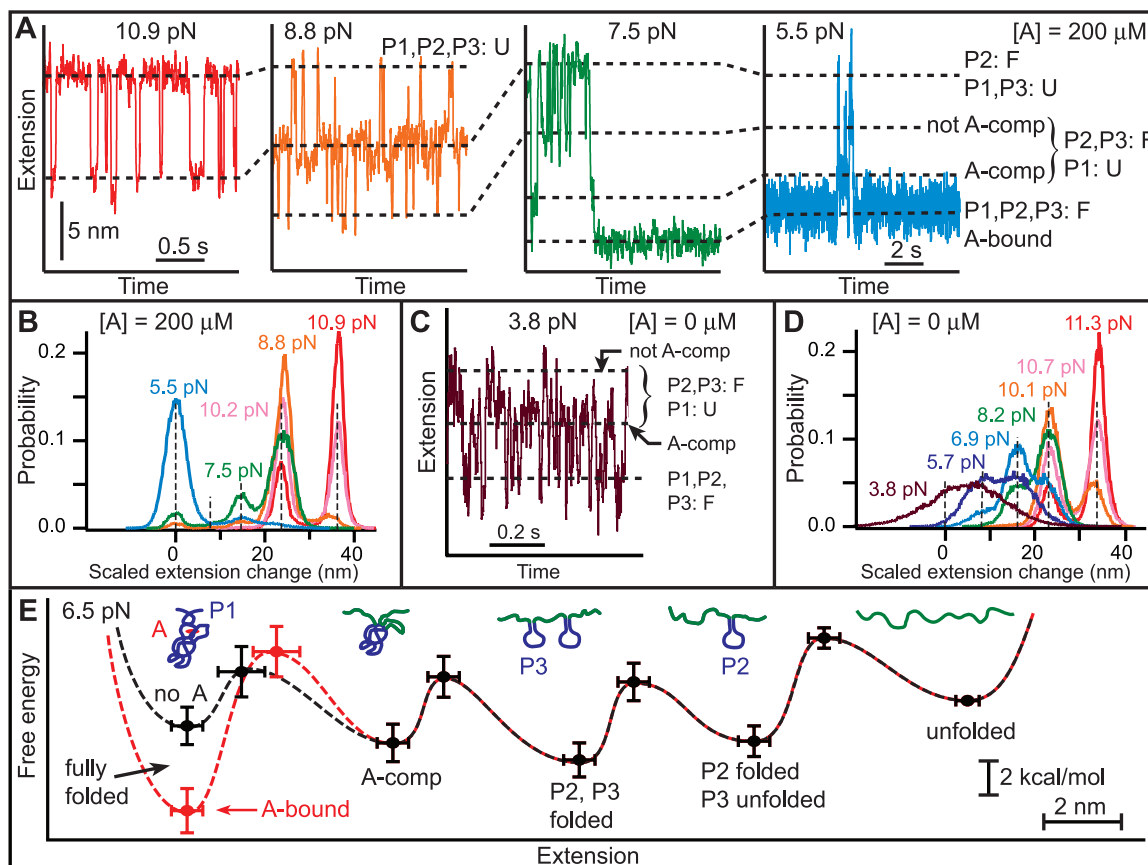
interactions creating the binding pocket; hence, we model this process using just three distinct states. A global fit of data to the time-dependent folding probabilities returned $k_1 = 0.4 \pm 0.05\ \mathrm{s}^{-1}$, $k_{\mathrm{off}} = 0.2 \pm 0.05\ \mathrm{s}^{-1}$, and $k_{\mathrm{on}} = 8 \pm 1 \times 10^4\ \mathrm{M}^{-1}\ \mathrm{s}^{-1}$. The value of k_{off} is similar to that obtained above, and k_{on} is close to the value measured by bulk experiments (12). The slow folding rate implies that both aptamer folding and adenine binding occur on the same time scale as transcription itself, supporting the hypothesis that the function of this riboswitch is governed by folding and binding kinetics rather than equilibrium thermodynamics (10, 26).

The multiple steps in the overall folding reaction were studied in greater detail by unfolding the aptamer completely and monitoring its extension under constant force with a passive force clamp (27) as the force was reduced stepwise every 1 to 2 min. Observing the transitions in the refolding process individually, based on their different energies and time scales, four distinct steps were seen (Fig. 4). The first folding event, at ~9 to 11 pN (Fig. 4A, red), involves length changes and force-dependent kinetics consistent with folding the 21-nt hairpin P2, as predicted by an energy landscape model for hairpin folding (16, 18). The second folding step, at ~7 to 8 pN (Fig. 4A, orange), matches the properties expected for folding the 19-nt hairpin P3. The identification of these steps with the folding of P2 and P3 was confirmed by blocking the folding of each hairpin separately with antisense oligomers (fig. S3). We speculate that P2, the first fully transcribed element, is also the most stable in order to ensure that it can form in the presence of competing, alternative secondary structures in the upstream mRNA that might delay or prevent the formation of the proper aptamer structure.

In contrast to the adenine-independent events described above, the two folding transitions observed at lower forces were found to be adenine-dependent. For forces below ~7 pN at saturating adenine concentrations, the aptamer spent considerable time in the shortest-extension state (Fig. 4A, green and blue), which we identify as the folded, adenine-bound state. That identification was confirmed by measuring a contour length change of 63 ± 1 nt when the 63-nt aptamer was completely unfolded from this state. The contour length change between this state and the one with only P2 and P3 folded, 21 ± 2 nt, is consistent with the 23 nt that are not involved in P2 and P3 folding. In addition, a transient intermediate was observed between these two states, 14 ± 1 nt from the folded state. Because there are 15 nt in and adjacent to P1 (Fig. 1A), we identify this intermediate as a state where P2 and P3 are folded and the adenine binding pocket is preorganized by tertiary contacts, sequestering the nucleotides between P2 and P3, but P1 remains unfolded. The extensions of all five states (fully unfolded, P2 folded, P2/P3 folded, P1 unfolded, and fully folded), scaled by the fractional extension per nucleotide at a given force, are evident in histograms of records (Fig. 4B).

Constant-force–extension records in the absence of adenine (Fig. 4, C and D) indicate very different behavior at low forces: The P1-unfolded state is strongly populated below ~6 pN, whereas the folded state is only well populated below ~4 pN. Even at such low forces, the folded-state lifetime is short, with a rapid equilibrium between folded and P1-unfolded states. These differences can be understood if the P1-unfolded state is the adenine-competent state. At saturating adenine concentrations, the formation of this state leads rapidly to an adenine-bound, folded state that is long-lived even at ~7 pN (Fig. 4A), and the P1-unfolded state is thus rarely occupied. In contrast, absent adenine, the P1-unfolded state is frequently occupied even at low forces. Occasionally, the transient folding of P1 was observed even with adenine present (Fig. 4A, green), likely indicating that adenine was not bound at that instant. The single-molecule records thus directly reflect an adenine-induced stabilization of helix P1 that underpins the switching action of the riboswitch (28).

Each of the folding transitions can be analyzed individually as a two-state process, enabling a piecewise reconstruction of the energy landscape for folding, both with and without adenine (Fig. 4E). The relative free energies of the five observed states were determined from extension histograms, and the locations and heights of the energy barriers between states were determined from the force dependence of the kinetics (15, 18). From these landscapes, we find that the tertiary contacts that form the adenine-competent state, which are primarily base-pair and base-quartet interactions between hairpin loops (4, 9), stabilize the structure by an additional 2.7 ± 0.3 kcal/mol (18). The transition state for breaking these interactions lies ~1 nm from the adenine-competent state, indicative of their short range (29). We also find that adenine binding stabilizes the folded state by 4 ± 1 kcal/mol, but does not appreciably affect other properties of the landscape.

These energy landscapes dramatically illustrate the sequential folding of each structural element in the RNA. Folding proceeds through a distinct hierarchy of states, but the formation of tertiary and secondary structure is interleaved, because the energetic stabilities of these structures happen to be comparable, in contrast with the standard picture of hierarchical folding. Indeed, the tertiary contacts that preorganize the adenine-competent state are considerably more stable than the least-stable helix, P1, which is the essential component governing the switching behavior of the riboswitch. In vivo, without adenine binding to stabilize P1, this last component of the aptamer to fold would be highly susceptible to disruption by terminator hairpin invasion.

The techniques developed here point the way to a powerful method for monitoring cotranscriptional folding. In the case of the *pbuE* aptamer, the first FEC obtained after transcription did not exhibit an unfolding behavior substantially different from that of subsequent FECs, implying that the cotranscriptional aspect of folding may not be important for the formation of an isolated aptamer (18). This result is unsurprising, because structural elements of the aptamer fold in the same order as they are transcribed; hence, force-induced refolding mimics cotranscriptional folding in this case. However, for the folding of the complete riboswitch, which includes a downstream terminator hairpin that competes with aptamer formation, we anticipate an important cotranscriptional dependence (10, 26).

References and Notes

1. W. C. Winkler, R. R. Breaker, *Annu. Rev. Microbiol.* **59**, 487 (2005).
2. R. L. Coppins, K. B. Hall, E. A. Groisman, *Curr. Opin. Microbiol.* **10**, 176 (2007).
3. R. T. Batey, S. D. Gilbert, R. K. Montange, *Nature* **432**, 411 (2004).
4. A. Serganov et al., *Chem. Biol.* **11**, 1729 (2004).
5. M. Mandal et al., *Cell* **113**, 577 (2003).
6. J. Noeske et al., *Proc. Natl. Acad. Sci. U.S.A.* **102**, 1372 (2005).
7. S. D. Gilbert, C. D. Stoddard, S. J. Wise, R. T. Batey, *J. Mol. Biol.* **359**, 754 (2006).
8. J. Noeske et al., *Nucleic Acids Res.* **35**, 572 (2007).
9. O. M. Ottink et al., *RNA* **13**, 2202 (2007).
10. J. F. Lemay et al., *Chem. Biol.* **13**, 857 (2006).
11. M. Mandal, R. R. Breaker, *Nat. Struct. Mol. Biol.* **11**, 29 (2004).
12. J. K. Wickiser, M. T. Cheah, R. R. Breaker, D. M. Crothers, *Biochemistry* **44**, 13404 (2005).
13. E. A. Abbondanzieri, W. J. Greenleaf, J. W. Shaevitz, R. Landick, S. M. Block, *Nature* **438**, 460 (2005).
14. I. Tinoco Jr., C. Bustamante, *Biophys. Chem.* **101-102**, 513 (2002).
15. M. T. Woodside et al., *Science* **314**, 1001 (2006).
16. M. T. Woodside et al., *Proc. Natl. Acad. Sci. U.S.A.* **103**, 6190 (2006).
17. R. V. Dalal et al., *Mol. Cell* **23**, 231 (2006).
18. Materials and methods are available as supporting material on *Science* Online.
19. B. Onoa et al., *Science* **299**, 1892 (2003).
20. O. K. Dudko, G. Hummer, A. Szabo, *Phys. Rev. Lett.* **96**, 108101 (2006).
21. S. B. Smith, Y. Cui, C. Bustamante, *Science* **271**, 795 (1996).
22. Y. Seol, G. M. Skinner, K. Visscher, *Phys. Rev. Lett.* **93**, 118102 (2004).
23. W. Saenger, *Principles of Nucleic Acid Structure* (Springer, New York, 1984).
24. J. Liphardt, S. Dumont, S. B. Smith, I. Tinoco Jr., C. Bustamante, *Science* **296**, 1832 (2002).
25. C. Jarzynski, *Phys. Rev. Lett.* **78**, 2690 (1997).
26. J. K. Wickiser, W. C. Winkler, R. R. Breaker, D. M. Crothers, *Mol. Cell* **18**, 49 (2005).
27. W. J. Greenleaf et al., *Phys. Rev. Lett.* **95**, 208102 (2005).
28. Some molecular heterogeneity was present, but we did not observe order-of-magnitude variations in the kinetics from one RNA to the next, as reported in one single-molecule fluorescence study (10).
29. P. T. X. Li, C. Bustamante, I. Tinoco Jr., *Proc. Natl. Acad. Sci. U.S.A.* **103**, 15847 (2006).
30. We thank R. Landick for providing purified RNAP, K. Herbert for providing the plasmid used to make the transcription template, M. Larson and O. Dudko for helpful advice, and members of the Block lab and Program Project grant GM066275 for useful discussions. Our research was supported by grants from the National Institute of General Medical Sciences (GM057035) and the National Institute for Nanotechnology.